10^{th} International Conference on Fracture Mechanics of Concrete and Concrete Structures
FraMCoS-X
G. Pijaudier-Cabot, P. Grassl and C. La Borderie (Eds)
https://doi.org/10.21012/FC10.235566

SIMULATION OF PUSH-OUT TESTS OF CORRODED REINFORCED CONCRETE SPECIMENS BY MEANS OF COHESIVE INTERFACE ELEMENTS WITH FRICTIONAL BEHAVIOR

BEATRIZ SANZ*, JAIME PLANAS† AND JOSÉ M. SANCHO‡

*Universidad Politécnica de Madrid, ETSI Caminos, Canales y Puertos, Profesor Aranguren 3, Madrid, Spain
e-mail: beatriz.sanz@upm.es

†Universidad Politécnica de Madrid, ETSI Caminos, Canales y Puertos, Profesor Aranguren 3, Madrid, Spain
e-mail: jaime.planas@upm.es

‡ Universidad Politécnica de Madrid, ETS de Arquitectura, Avda. Juan de Herrera 3, Madrid, Spain
e-mail: jose.sancho@upm.es

Key words: Reinforced Concrete, Bond, Cohesive Crack, Corrosion

Abstract. Loss of bond between steel and concrete is one of the effects of corrosion of reinforced concrete specimens. In order to study that, push-out tests were designed and carried out in previous works, in which the specimens were slices cut from concrete prisms reinforced with a smooth steel tube. This allows adhesion and friction to be investigated, avoiding influence of bar deformations on bond stress. The prisms were subjected to accelerated corrosion tests within the framework of a general study of cracking of concrete due to reinforcement corrosion, as presented in previous conferences. In this work simulation of the bond tests has been carried out in order to study numerically the effect of adherence and friction, by using three-dimensional models of the specimens. The simulations have been carried out within the finite element framework COFE (Continuum Oriented Finite Element), which implements elements with an embedded adaptable crack to reproduce fracture of concrete according to the standard cohesive model. Additionally, joint elements with cohesive softening and friction have been programmed to reproduce the behavior of the steel-concrete interface. The numerical and experimental results of specimens not subjected to accelerated corrosion show a good agreement, which confirms that a cohesive-frictional law is adequate to reproduce the interface behavior. In addition, the effect of adhesion and friction on bond has been studied separately in the simulations. In the paper, the main aspects of the push-out tests are introduced, formulation of the joint elements is presented, and the numerical and experimental results are analyzed, with special focus on the numerical aspects of the constitutive law of the joint elements.

1 INTRODUCTION

Loss of bond between steel and concrete is one of the main consequences of corrosion of the reinforcement. The studies found in the literature show that for specimens with a high degree of corrosion the maximum bond strength decreases due to the lubricant effect of the generated oxide layer, degradation of the bar ribs and propagation of longitudinal cracks which diminishes confinement [1, 2]. Moreover, degradation of stirrups might influence bond strength as well, since they are the main mechanism of confinement after cracking of the cover [3,4]. However, influence of corrosion on each factor contributing to bond strength is not

quantified, due to the difficulty to decouple the effect of those in experiments.

In order to study loss of bond due to reinforcement corrosion, the authors of this work designed an experimental device for *push-out* tests, in which a steel tube embedded in a concrete slice is pushed out from that [5]. This allows adhesion and friction to be investigated, avoiding influence of the steel deformations, as interlocking of bar deformations against the concrete does not occur. The specimens are slices cut from concrete prisms which were subjected to accelerated corrosion tests within the framework of a general study about cracking of concrete due to reinforcement corrosion [6, 7]. Tests were also performed for slices of specimens not subjected to accelerated corrosion. The push-out tests manifested that friction and confinement of the specimens are essential on bond stress once adhesion between the steel and the concrete is lost.

In a preliminar numerical study it was assessed by means of finite element simulations that the stress at the steel-concrete interface in push-out tests is uniform [8], thus verifying that the shear stress obtained from the results of this type of experiment is reliable.

The present work is a continuation of the mentioned numerical study and focus on the friction between the steel and the concrete. A frictional model with inelastic displacement has been implemented within the finite element framework COFE (*Continuum Oriented Finite Element*). Several strategies of superposition of frictional elements with cohesive elements have been investigated, in order to reproduce the behavior observed in the experiments. This study is limited to specimens without corrosion, as the previous step to the simulation of push-out tests of corroded specimens, for which it is planned to superpose a model that reproduces the mechanical behavior of the oxide layer.

In the current paper, Sec. 2 reviews the background of this work, Sec. 3 presents the main aspects of the model, Sec. 4 discusses the numerical results, advantages and limitations of the strategies of simulation of this work and Sec. 5 includes the conclusions.

2 BACKGROUND

2.1 Geometry of the specimens

The specimens are slices obtained from concrete prisms with an embedded calibrated steel tube. Figure 1 displays a sketch of the geometry of the slices.

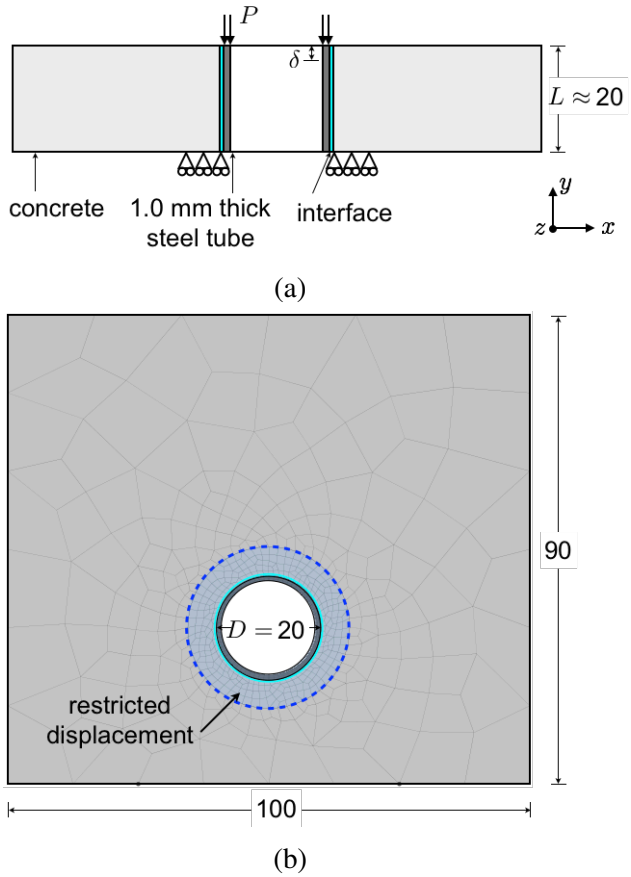

Figure 1: Geometry of the specimens of push-out tests, with dimensions in mm, and sketch of the test. In the figure, the mesh and boundary conditions of numerical simulations of the tests are sketched

The original prisms were subjected to accelerated corrosion tests using the experimental device presented in [6] in such conditions that a uniform oxide layer developed surrounding the steel tube and a main crack grew at the cover. Other secondary cracks developed surrounding the reinforcement, but they were much thinner than the main crack. A constant current of 400 $\mu A/cm^2$ was applied using the impressed current technique [9, 10]. Then the prisms were cut into slices with an average

thickness of 20 mm (see [5] for details in the slices preparation). A smooth steel tube was used as the reinforcement instead of a ribbed bar in order to perform special measurements during the accelerated corrosion tests, which provided relevant information about the mechanical behavior of the oxide.

2.2 Push-out tests

The design of push-out tests was conditioned by the geometry of the specimens, as anchoring of the tube was not possible. A *push-out* device was selected as the best solution for these specimens to push the tube out of the concrete. This device allows adhesion and friction to be studied, avoiding influence of the geometry of the bar ribs on the measured shear stress. For details in the experimental design see [11].

The tests were carried out under displacement control. The applied load P and the displacement of the tube δ were recorded during the test. Figure 1 shows a sketch of push-out tests and Fig. 2 a picture of the experimental device. For details in the test procedure, see [5]. The shear stress τ transmitted at the steel-concrete interface was computed taking into account the actual surface of concrete contacting the tube and assuming uniform stress along the tube length, as

$$\tau = \frac{P}{\pi D(L-\delta)} \qquad (1)$$

where P is the load, D is the outer diameter of the steel tube (i.e. 20 mm), L the average length of the tube, and δ the displacement of the tube.

Figure 3 shows typical curves of nominal shear stress versus displacement of the steel tube which were obtained for specimens not subjected to accelerated corrosion.

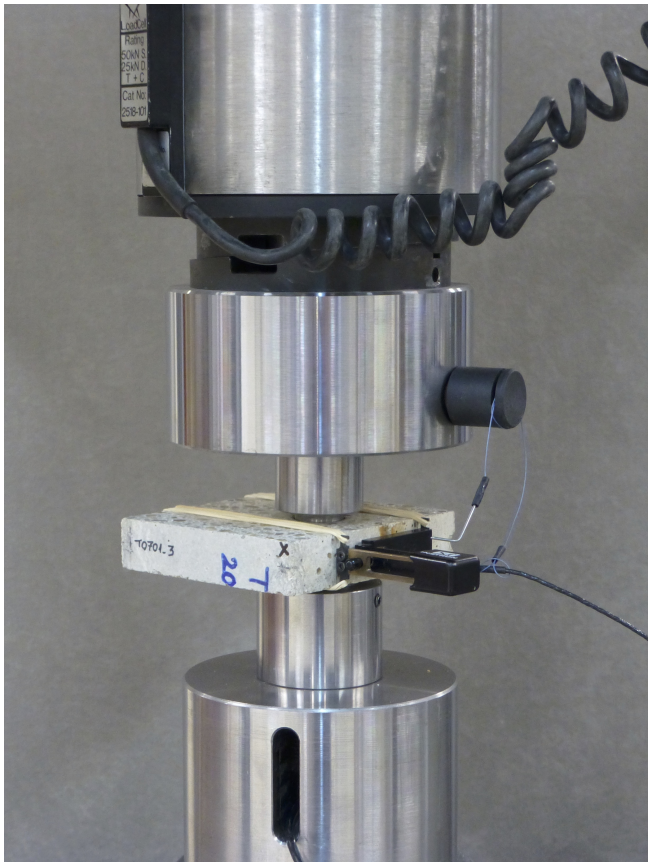

Figure 2: Experimental device for push-out tests

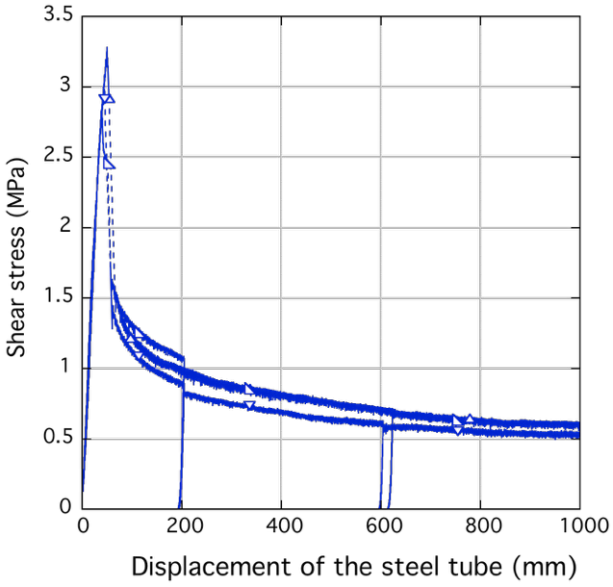

Figure 3: Results of push-out tests of specimens not subjected to accelerated corrosion

The curves are plotted up to a displacement of 1000 µm although the tests were run

for a greater displacement, since no significant changes occurred from that displacement on. The curves display an initial steep slope up to a peak; then there is a sudden drop with a marked instability, as indicated in the curves by the dotted lines, followed by a progressive descent of the stress until the end of the test, which indicates that there is a residual bond stress due to friction. Unload and reload branches were carried out, which manifested that the displacement of the tube is permanent after the peak load is reached. This motivated the implementation of a model with friction and permanent displacement in this work.

The results of specimens subjected to accelerated corrosion were very similar, except that the decrease in stress was progressive during the test. The residual stress depended on the corrosion level of the specimens. Moreover, an influence of the crack width on the residual stress was observed, manifesting influence of the confinement of the specimens on the shear stress after the peak load, which motivated as well implementation of the model presented in this paper.

2.3 Preliminar numerical study

The simulations of the present study and the previous one were carried out within the finite element framework COFE. Three-dimensional models have been used, which are described in Sec. 4.1. The finite element program implements elements with an embedded adaptable crack [12, 13] which reproduce the fracture behavior of concrete according to the cohesive model [14]. Those will be applied in future numerical simulations of push-out tests of corroded specimens. However, in this study concrete was assumed to be linear elastic, since the behavior of non-corroded slices, which are uncracked, have been simulated.

In order to simulate the behavior of the steel-concrete interface, *joint elements* have been used. Those are an extended version of the elements presented in [15]. Their main aspects are included here for completeness of the text. They are zero-thickness elements that transmit stress only between pairs of nodes and are defined by the external unitary normal **n** to the element. At their initial version, the joint elements were formulated for two-dimensional problems and were used to reproduce the mechanical behavior of the oxide layer. At their current version, formulation of the elements have been extended, leading to families of prisms and hypercubes which can be used in two- and three-dimensional problems. Figure 4 shows a sketch of the families of joint elements.

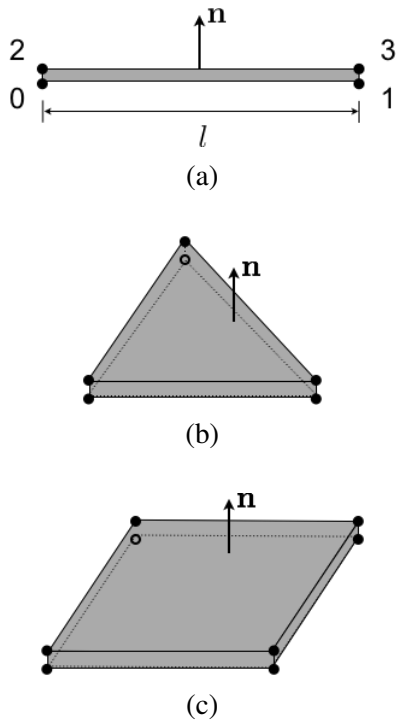

Figure 4: Sketch of the joint elements: two-dimensional element (a), prismatic element (b) and hexahedral element (c)

In the joint elements the traction vector **t** is computed from the displacement vector **w** considering the behavior in normal and shear direction by means of the corresponding stiffnesses as

$$\mathbf{t} = k_n(\mathbf{w}\cdot\mathbf{n})\mathbf{n} + k_s[\mathbf{w} - (\mathbf{w}\cdot\mathbf{w})\mathbf{n}] \quad (2)$$

where k_n is the normal stiffness, k_s the shear stiffness, **n** the unitary normal of the element, and **1** is the second order identity tensor.

For the preliminar study several cohesive laws were implemented, based on the damage model from Camanho and Davila [16], which

is sketched in Fig. 5(a). In that model, stiffness degrades as a function of the maximum displacement, with unloading to the origin.

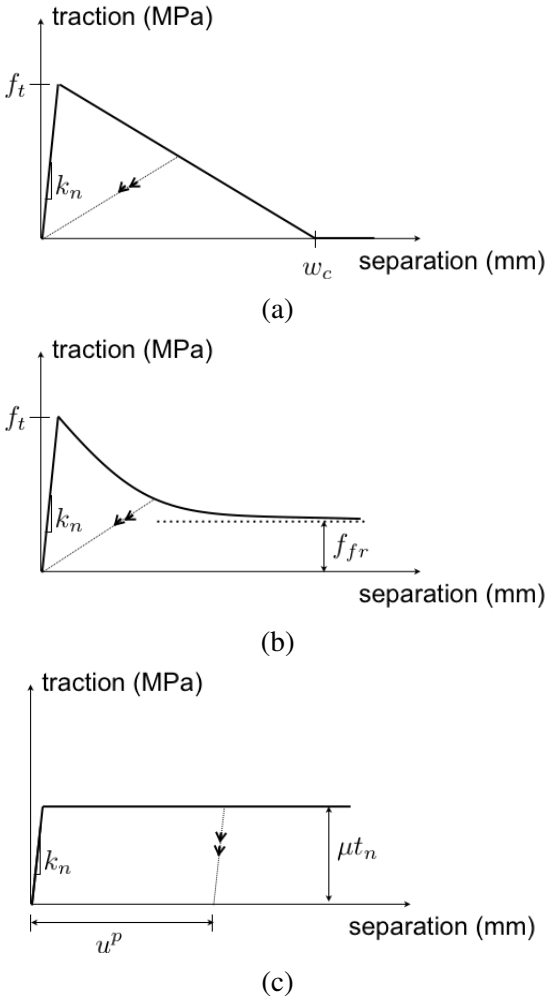

Figure 5: Models for joint elements: cohesive law with linear softening based on the model from Camanho y Davila [16] (a) and exponential law (b), used in preliminar calculations [8], and friction model with inelastic displacement (c) programmed in the current study.

In particular, three laws were implemented: the first one with linear softening, the second one with linear softening plus constant friction after a given displacement, and the third one with exponential softening and asymptote with a given value f_{fr}. In all the cases, an equivalent displacement w_m is considered, which includes the positive normal displacement $\langle \mathbf{w}_n \rangle$, i.e., the displacement in the case of tension, and the shear displacement w_s:

$$\mathbf{w}_m = \mathbf{w}_s + \langle \mathbf{w}_n \rangle \tag{3}$$

For the negative normal displacement, i.e., the displacement in compression, linear elastic behavior is assumed.

In the numerical study push-out tests of specimens not subjected to accelerated corrosion was simulated by using the mentioned three models. It was verified that the shear stress at the steel-concrete interface is uniform after the peak load, thus, assessing the validity of the test of push-out for studying bond stress.

The cohesive law with exponential softening (see sketch in Fig. 5b) was the best to reproduce the behavior observed in the experiments. However, this law has the limitation that the residual friction at the end of the test was a constant imposed value, while in the experiments it was observed that the final stress depends on the crack width, thus, manifesting influence of the confinement. This motivated implementation of the model described in the next section.

3 FRICTION MODEL WITH INELASTIC DISPLACEMENT

In this work a model with frictional behavior and inelastic displacement has been programmed, as sketched in Fig. 5(c), with the following basis.

Let us consider $\mathbf{K}$ the elastic stiffness tensor of the element

$$\mathbf{K} = k\mathbf{1} \tag{4}$$

where $\mathbf{1}$ is the second order identity tensor and k a fictitious stiffness, which is necessary to avoid numerical instabilities. For a given displacement vector $\mathbf{u}$ applied to the element, $\mathbf{u}^p$ is the plastic displacement vector due to slide. Then the traction vector $\mathbf{t}$ of the element is calculated as

$$\mathbf{t} = \mathbf{K}(\mathbf{u} - \mathbf{u}^p) \tag{5}$$

with the assumption that $\mathbf{u}^p$ is perpendicular to the normal direction of the displacement. The criterium for initiation of inelastic displacement is

$$|\mathbf{t}_s| - \mu p \leq 0 \tag{6}$$

where $\mathbf{t}_s$ is the shear component of the traction vector, μ the friction coefficient which depends

on the material, and p the modulus of the normal component of the traction vector. If Eq. (6) is true, then the displacement is elastic. Otherwise, there is plastic displacement and the shear component of the traction vector is limited to the value of μp.

At the programming level, this limitation of the shear component of the traction vector implies a correction of the inelastic displacement of the previous step with a radial return displacement $\delta\mathbf{u}^p$.

Figure 6 displays the results of an example with a unique element. This is an hexahedron with stiffness k=100 N/mm^{3}m and friction coefficient μ=0.4 (model Friction 1 in Table 4.1). An increasing shear displacement up to 0.02 mm, then decreasing up to 0.01 mm and then increasing again up to 0.025 mm is applied to each node of the upper side of the element, while the displacement of the remaining nodes is zero. A normal force of -0.1 N is also applied at each upper node in oder to ensure compression of the element. As shown in the figure, the resulting shear force coincides with the theoretical corresponding to the conditions of this problem.

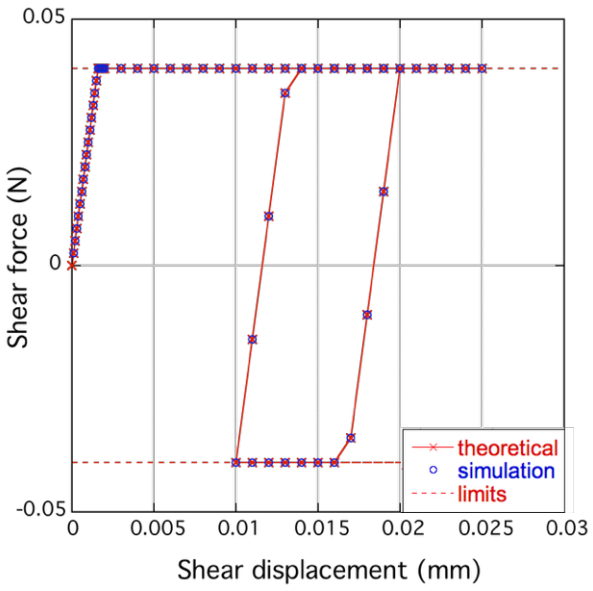

Figure 6: Results of a numerical test of the frictional model with inelastic displacement

4 NUMERICAL STUDY

4.1 Characteristics of the simulations

Simulations have been carried out by using two three-dimensional models: the first one with an only hexahedral element with a cross-sectional area of $1 \times 1\,\text{mm}^2$, which has been used for verifications, and the second one which reproduces the geometry of the slices and the boundary conditions of push-out tests. The characteristics of this last model are described in the following.

Figure 1 displays a sketch of the mesh and boundary conditions applied in the simulations. A structured mesh as that described in [8] was used, which was generated by using the pre-post Finite Elements mesh processor Gmsh [17]. Hexahedral elements with assumed enhanced strain were used for the steel and concrete elements, and joint elements of type hexahedra for the interface. The number of hexahedra in the direction of the thickness of the slice was eight. In the plane of the cross-section, the number of interface and steel elements per quarter of circumference was sixteen, with one layer of joint elements and three layers of steel elements. The mesh of the concrete matched the mesh of the tube. The size of the elements at the outer boundary of the concrete was increased to be ten times that of the interface elements.

A vertical displacement was imposed at the upper nodes of the steel tube. The displacement was restricted at the nodes of the bottom side of concrete of the shadowed zone, which corresponds the device that supports the concrete slice in the experiments (see [5]). In addition, the displacement of two nodes of the bottom side of concrete was restricted for the sake of a proper conditioning of the numerical problem.

The resulting stress at the interface was computed from the sum of the nodal reaction of the nodes of concrete with restricted displacement, assuming uniform stress, as in the experiments.

Table 4.1 displays the reference values of the parameters of the materials. For the steel and concrete, linear elastic behavior was assumed, with standard parameters, as in [8]. For the

Table 1: Reference parameters of the materials, where E is the elastic modulus, ν Poisson's ratio, α the thermal expansion factor, k the fictitious stiffness, μ the friction coefficient, f_t the tensile strength, w_{c2} the displacement for which the stress of the cohesive law is zero, measured from the displacement of the peak, c and f_{fr} are the exponent and the asymptotic value of the exponential cohesive law, respectively, Lin. soft. stands for linear softening, and Exp. soft. stands for exponential softening

	E (GPa)	ν	α	k (N/mm^3)	μ	f_t (MPa)	w_{c2} (mm)	c (mm^{-1})	f_{fr} (MPa)
Concrete	30	0.2	10^{-5}	—	—	—	—	—	—
Steel	200	0.3	0.0	—	—	—	—	—	—
Friction 1	—	—	—	100	0.4	—	—	—	—
Friction 2	—	—	—	1000	0.4	—	—	—	—
Lin. soft.	—	—	—	100	—	1	0.3	—	—
Exp. soft.	—	—	—	1000	—	3	—	25	0.0

concrete a thermal expansion factor was considered, in order to simulate a strain equivalent to its retraction. For the joint elements several laws were used: frictional law with inelastic displacement with the values displayed for Friction 1 and Friction 2, cohesive law with linear softening and cohesive law with exponential softening. See Fig. 5 for the physical meaning of the parameters of the laws for joint elements.

4.2 Simulations with friction and retraction

Preliminar simulations of push-out tests have been carried out to verify the effect of friction. As reference parameters, the values of model Friction 2 displayed in Table 4.1 have been used. Simulations have been carried out as well with a friction coefficient equal to 0.2 and keeping the remaining parameters.

A thermal strain was imposed to the concrete elements to simulate the effect of retraction, in order to ensure compression at the steel-concrete interface. In particular, negative increments of temperature r were imposed bewteen -5ºC and -50ºC, which produce strains of $-5 \cdot 10^5$ y $-5 \cdot 10^{-4}$. Those values are among the normal ranges of strain due to retraction, as reported in the Spanish Standard of Structural Concrete [18]. A total displacement of 10 μm was imposed to the steel tube in nine steps, except for the simulation with $r = 5$ºC in which it was applied in ten steps, in order to capture initiation of sliding. Prior to that, the thermal strain was applied in one step.

Figure 7 displays the curves of shear stress versus displacement of the steel tube.

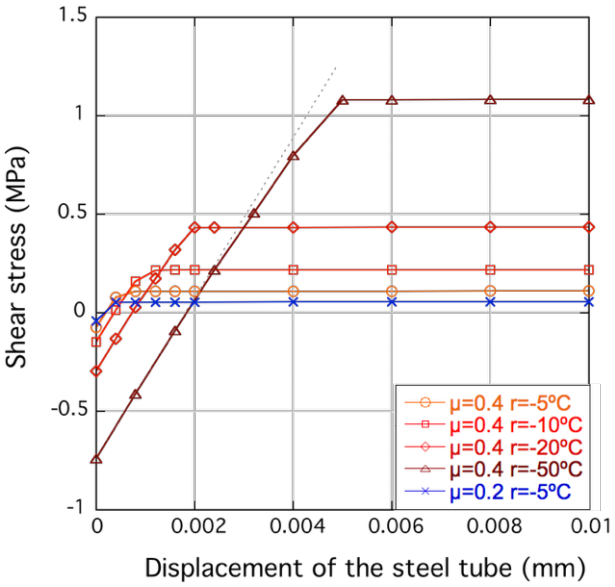

Figure 7: Simulation of push-out tests with retraction, considering a model with friction and inelastic displacement

It is observed that a greater retraction increases the shear stress, due to the increment in the normal stress of the interface. The effect of an increase in the friction coefficient is similar. However, the curves differ from those obtained in the experiments, as these examples only include the effect of friction. Thus results of simulations considering a cohesive effect to simulate adhesion are shown in the subsequent sections.

It should be noticed that the negative stress obtained for the initial step in all the simulations is due to the boundary conditions of the problem. Retraction is simulated as a negative increment of temperature which is applied to the concrete nodes, not to the steel nodes, while displacement is restricted in some nodes of the bottom face of concrete and some nodes of the upper side of steel (see Sec. 4.1). In particular, for the first step, the displacement of the upper steel nodes is zero, which introduces a fictitious relative displacement between the steel and the concrete, with a negative reaction in the concrete. This effect is more noticeable for the cases with greater retraction and friction coefficient.

Figure 8 shows an example of the map of normal stress and shear stress obtained at the final step for a simulation with μ=0.4 y r=-5ºC. It should be noticed that there is a tridimensional effect as manifested in those maps.

4.3 Superposition of models

In order combine the effect of friction with that of a cohesive law, the solution in this work has been to superpose two layers of elements which share nodes, each layer with the corresponding constitutive model. It entails that nodal displacement of the elements is the same and the nodal forces calculated for each element are added.

A verification example has been carried out by using a model with two superposed interface elements. The same conditions as in the example described in Sec. 3 have been applied. For the element with frictional behavior, the parameters of model Friction 1 displayed in Table 4.1 have been used, and for the element with cohesive behavior the parameters of model Lin. Soft., which stands for linear softening. Simulations have been run as well for each element individually. Figure 9 displays the curves of shear force versus displacement for the model with superposed elements and for each individual model. It is verified that the behavior of the model with superposed elements coincides with the sum of the response of the individual elements.

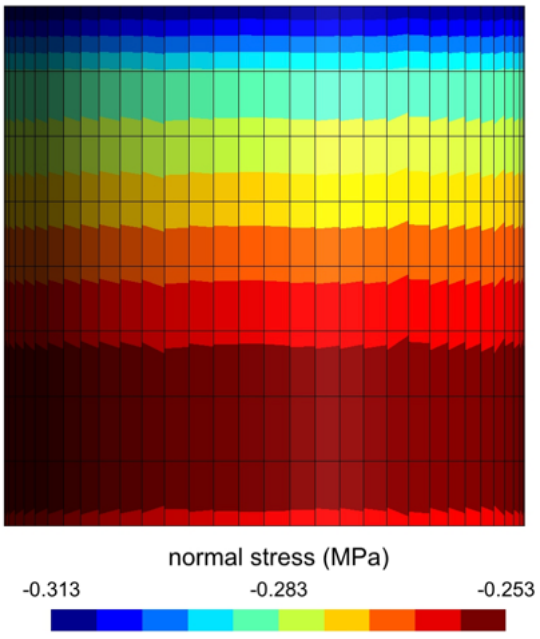

(a)

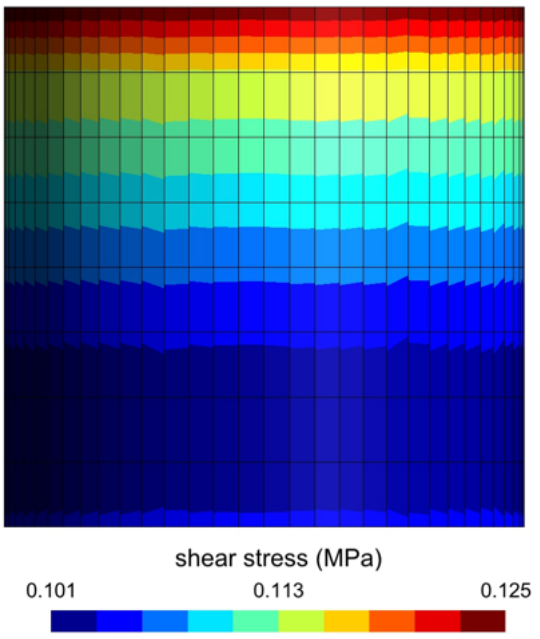

(b)

Figure 8: Map of normal stress (a) and map of shear stress (b) obtained at the interface for a displacement of the tube of 0.01 mm for a simulation with μ=0.4 y r=-5ºC.

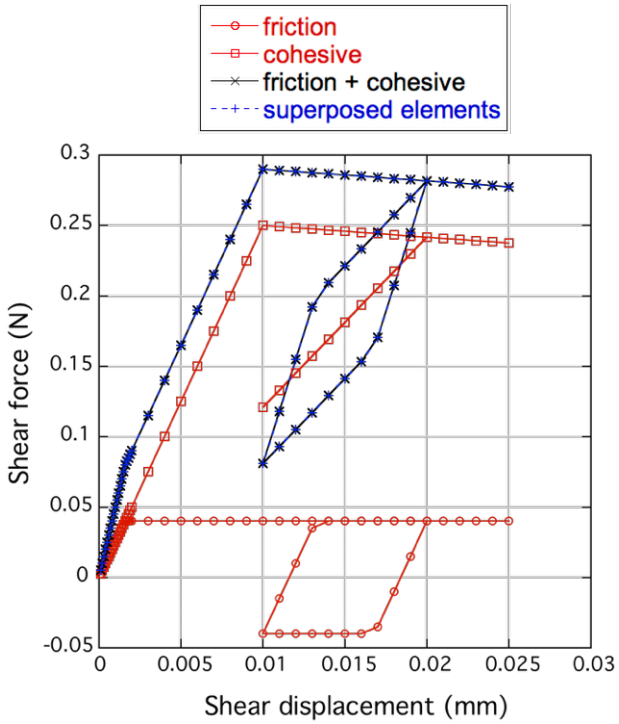

Figure 9: Resultado de un ensayo numérico de la superposición de dos elementos junta.

It should be noticed that when applying a normal force at the nodes instead of a normal displacement in order to ensure compression of the element, the coupled elements require double force than the individual elements, as stiffnesses of the elements are summed and the resulting normal displacement is smaller. It should also be noticed that in the coupled model implies an increase in the number of elements, which could be significant for fine meshes, with the subsequent increase in the time of computation. For that reason, a model with incorpores the two behaviors, friction and cohesive, will be programmed in the future, as an alternative to the superposition of elements.

4.4 Simulation of push-out tests

As final application of this work, push-out tests have been simulated for specimens not subjected to accelerated corrosion, superposing to layers of joint elements between the steel and the concrete. The first layer of elements has the characteristics of model Friction 2 displayed in Table 4.1 and the second layer those of model Exp. Soft, which stands for exponential softening. In addition, simulations with an exponent $c = 12.5\,\mathrm{mm}^{-1}$ and the remaining parameters as in model Exp. Soft. have been carried out. In the simulation increments of temperature between -5ºC and -50ºC have been applied in order to simulate retraction.

Figure 10 shows the resulting curves of shear stress versus displacement of the steel tube. It is observed that the simulated curves reproduce the experimental results (see Fig. 3), although no attempt has been done in this work to obtain the best values for the parameters. It should be noticed, however, that implementation of the friction model with inelastic displacement entails an improvement with respect to the law with exponential softening and residual strength, since this model reproduces the stress at the end of the test by taking into account the parameters of the material. Moreover, it takes into account the effect of confinement by means of the variations in the normal stress, which will be applied in the future to study bond behavior of corroded specimens.

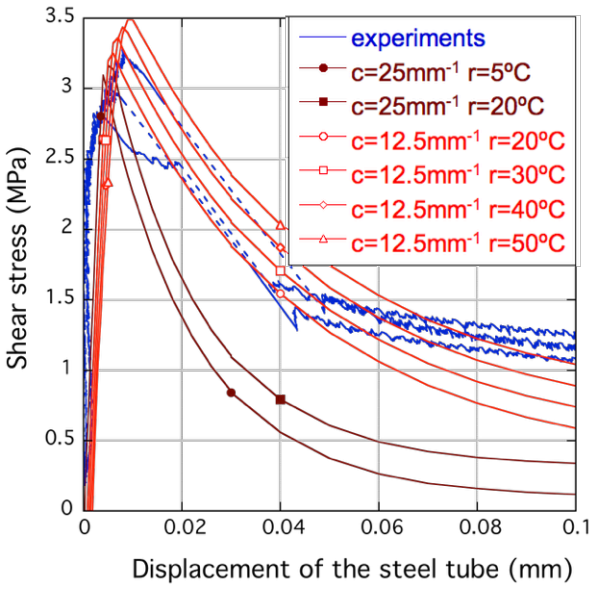

Figure 10: Simulation of push-out tests with retraction, considering a model with friction and inelastic displacement coupled with a cohesive model with exponential softening

5 CONCLUSIONS

A model has been programmed that reproduces friction and inelastic displacement. The superposition of this one and a cohesive model reproduces the curves of shear displacement versus displacement obtained in push-out tests of specimens not subjected to accelerated corrosion. This model takes into account the effect of the normal stress of the element, which will be applied in the future to study bond behavior of corroded specimens.

A strategy of superposition has been used to obtain a coupled effect of the models with friction with inelastic displacement and cohesive behavior, with satisfactory results. In that, joint elements are duplicated and share nodes. It is planned to program a model incorporating both behaviors in order to avoid increasing the time of calculation in problems with fine meshes.

ACKNOWLEDGEMENTS

The authors gratefully acknowledge the *Secretaría de Estado de Investigación, Desarrollo e Innovación* of the Spanish *Ministerio de Economía y Competitividad* for providing financial support for this work under grant BIA2014-54916-R.

REFERENCES

[1] Al-Sulaimani, G.J., Kaleemullah, M., Basunbul, I.A., and Rasheeduzzafar, 1990. Influence of corrosion and cracking on bond behavior and strength of reinforced concrete members. *Structural Journal* **87**:220–231.

[2] Almusallam, A.A., Al-Gahtani, A.S., Aziz, A., and Rasheeduzzafar, 1996. Effect of reinforcement corrosion on bond strength. *Construction and Building Materials* **10**:123–129.

[3] Hanjari, K.Z., Coronelli, D., and Lundgren, K., 2011. *Modelling of Corroding Concrete Structures*, chapter Severely Corroded Reinforced Concrete with Cover Cracking: Part 2. Anchorage Capacity, pp. 207–217, Springer Netherlands, Dordrecht.

[4] Juarez, C., Guevara, B., Fajardo, G., and Castro-Borges, P., 2011. Ultimate and nominal shear strength in reinforced concrete beams deteriorated by corrosion. *Engineering Structures* **33**:3189–3196.

[5] Sanz, B., Planas, J., and Sancho, J., 2018. Study of the loss of bond in reinforced concrete specimens with accelerated corrosion by means of push-out tests. *Construction and Building Materials* **160**:598–609.

[6] Sanz, B., Planas, J., and Sancho, J., 2015. A closer look to the mechanical behavior of the oxide layer in concrete reinforcement corrosion. *International Journal of Solids and Structures* **62**:256–268.

[7] Sanz, B., Planas, J., and Sancho, J., 2016. An experimental and numerical method to investigate the oxide behavior in corrosion of reinforced concrete, in E.L. V. Saouma J. Bolander (Ed.), *Proceedings of the 9th International Conference on Fracture Mechanics of Concrete and Concrete Structures FraMCoS-9, Berkeley, USA*.

[8] Sanz, B., Planas, J., and Sancho, J., 2018. Simulation of interface behavior between steel and concrete to study loss of bond due to reinforcement corrosion, in G. Meschke, B. Pichler, and J.G. Rots (Eds.), *Computational Modelling of Concrete Structures*, pp. 785–794, CRC Press.

[9] Andrade, C., Alonso, C., and Molina, F.J., 1993. Cover cracking as a function of bar corrosion: Part i-experimental test. *Materials and Structures* **26**:453–464.

[10] El Maaddawy, T. and Soudki, K., 2003. Effectiveness of impressed current technique to simulate corrosion of steel reinforcement in concrete. *Journal of Materials in Civil Engineering* **15**:41–47.

[11] Sanz, B., 2014. *Experimental and numerical study of cracking of concrete due to reinforcement corrosion*, Ph.D. thesis, Universidad Politécnica de Madrid.

[12] Sancho, J.M., Planas, J., Cendon, D.A., Reyes, E., and Galvez, J.C., 2007. An embedded cohesive crack model for finite element analysis of concrete fracture. *Engineering Fracture Mechanics* **74**:75–86.

[13] Sancho, J., Planas, J., Fathy, A., Gálvez, J., and Cendón, D., 2007. Three-dimensional simulation of concrete fracture using embedded crack elements without enforcing crack path continuity. *International Journal for Numerical and Analytical Methods in Geomechanics* **31**:173–187.

[14] Hillerborg, A., Modéer, M., and Petersson, P.E., 1976. Analysis of crack formation and crack growth in concrete by means of fracture mechanics and finite elements. *Cement and Concrete Research* **6**:773–781.

[15] Sanz, B., Planas, J., and Sancho, J., 2013. An experimental and numerical study of the pattern of cracking of concrete due to steel reinforcement corrosion. *Engineering Fracture Mechanics* **114**:26–41.

[16] Camanho, P.P. and Davila, C.G., 2002. *Mixed-Mode Decohesion Finite Elements for the Simulation of Delamination in Composite Materials*, Technical report, NASA/TM-2002-211737, pp. 1–37.

[17] Geuzaine, C. and Remacle, J.F., 2009. Gmsh: a three-dimensional finite element mesh generator with built-in pre- and post-processing facilities. *International Journal for Numerical Methods in Engineering* **79**:1309–1331.

[18] EHE-08, 2008. *Instrucción de Hormigón Estructural*, Comisión Permanente de Hormigón, Ministerio de Fomento, publication in Spanish.